Journal of the Geological Society

Redistribution of the lithosphere deformation by the emplacement of underplated mafic bodies: implications for microcontinent formation

Tadashi Yamasaki and Laurent Gernigon

Journal of the Geological Society 2010; v. 167; p. 961-971
doi:10.1144/0016-76492010-027

Email alerting service click here to receive free email alerts when new articles cite this article

Permission request click here to seek permission to re-use all or part of this article

Subscribe click here to subscribe to Journal of the Geological Society or the Lyell Collection

Notes

Downloaded by University of Leeds on 23 August 2010

© 2010 Geological Society of London

Lyell Collection

Journal of the Geological Society, London, Vol. **167**, 2010, pp. 961–971. doi: 10.1144/0016-76492010-027.

Redistribution of the lithosphere deformation by the emplacement of underplated mafic bodies: implications for microcontinent formation

TADASHI YAMASAKI[1] & LAURENT GERNIGON[2]
[1]*School of Earth and Environment, University of Leeds, Leeds LS2 9JT, UK*
[2]*Geological Survey of Norway (NGU), Leiv Eirikssons vei 39, N-7491 Trondheim, Norway*
**Corresponding author (e-mail: t.yamasaki@leeds.ac.uk)*

Abstract: Sedimentary basin migration and microcontinent formation could be the result of deformation redistribution, in which the emplacement of an underplated mafic body (UPMB) may play an important role. In this study, a 2D finite-element model is used to examine the redistribution of the deformation that can be triggered by a UPMB. It is shown that three modes of deformation redistribution can exist: (1) a shift-completed mode where the deformation is completely redistributed into the newly weakened region; (2) a transition mode where the deformation is redistributed, but extension is accommodated by thinning in both regions; (3) a shift-failed mode where the deformation is not redistributed. Whether or not the deformation is redistributed depends on the configuration of the UPMB and on the initial rheological heterogeneity in the initially deformed region. However, it becomes difficult for any UPMB to initiate the redistribution of the deformation once the stretching factor in the first deformed region exceeds a critical value. The microcontinent formations observed in the Indian Ocean, in the Norwegian–Greenland Sea, in the Red Sea–Afar region and in the western Mediterranean are particularly discussed in relation to the transition mode, providing some important geodynamic implications.

In a system where forces are applied uniformly, a deformation is distributed into a particular region that has rheologically less strength. In such rheology-controlled deformation localization, which is different from that controlled by a locally applied force, the deformation could be redistributed into a different region if an additional weak zone is formed. This may be a fundamental concept that explains some geological phenomena including sedimentary basin migration and microcontinent formation.

Strengthening of the lithosphere in the extensional process is caused by thermal relaxation and replacement of weaker crust with stronger mantle, which has usually been considered as being responsible for causing successive deformation to migrate to adjacent regions (e.g. Braun 1992; Negredo *et al*. 1995; van Wijk & Cloetingh 2002; Corti *et al*. 2003*b*; Yamasaki & Gernigon 2009). However, the cessation, or at least a slow rate, of lithospheric thinning is required to obtain a significant strength contrast between extended and non-extended regions; otherwise the deformation is hardly redistributed. The condition of the mechanism is, therefore, so tightly limited that the strengthening does not work effectively when the thinning rate is fast enough to result in a large stretching factor of the lithosphere or in the onset of continental break-up.

Instead, the emplacement of underplated mafic bodies (UPMBs) can be an effective mechanism for deformation redistribution. Indeed, previous studies (Corti *et al*. 2002, 2003*a*, 2004; Yamasaki & Gernigon 2009) showed that the UPMB has a significant potential to bring about localization of the deformation, depending on its configuration (e.g. width, thickness and temperature) and on the thermal structure of the lithosphere into which the UPMB is emplaced. However, even though the UPMB ought to be formed by the magmatic activity that is controlled by the asthenosphere dynamics, the direct and intrinsic behaviour of the asthenosphere has not been well prescribed quantitatively and is still rather vague. Therefore, the nature of the UPMB's emplacement is uncertain; nevertheless, such an accidental thermal event, brought about by the asthenosphere dynamics, is a plausible controlling factor in the redistribution of deformation (e.g. Müller *et al*. 2001; Yamada & Nakada 2006; Mittelstaedt *et al*. 2008).

In this study, we examine the redistribution of deformation induced by the emplacement of a UPMB during extension. It is known that the deformation can be redistributed successfully if an additional weak zone is artificially introduced in some region. However, it still remains to evaluate the conditions required for the redistribution to occur. Mittelstaedt *et al*. (2008) has examined mid-ocean ridge jumps by means of a hotspot magma source, in which an abnormal heat source beneath a hot oceanic plate, as well as the magmatic intrusion in the plate, is imposed in a system where the sea floor is spreading at a constant rate. The present study, contrarily, describes the behaviour of the deformation redistribution on the condition that the UPMB-related weak zone is formed in the continental lithosphere before the initially deformed region develops into sea-floor spreading.

It is shown that there exist three modes of deformation redistribution, depending on the configuration of the UPMB's emplacement. The critical stretching factor in the first deformed region, below which the deformation localization can be redistributed into a different region where the UPMB is emplaced, is also evaluated. Then, based on the numerical model behaviour, we consider the implications for the microcontinent formations observed in the Indian Ocean, the Norwegian–Greenland Sea, the Afar–Red Sea region and the western Mediterranean Sea (see Fig. 1), including whether these natural example are suitable for the application of the model.

Model description

A 2D finite-element model is schematically depicted in Figure 2. The response of the three-layered continental lithosphere (wet quartzite upper crust, anorthite lower crust, and wet dunite

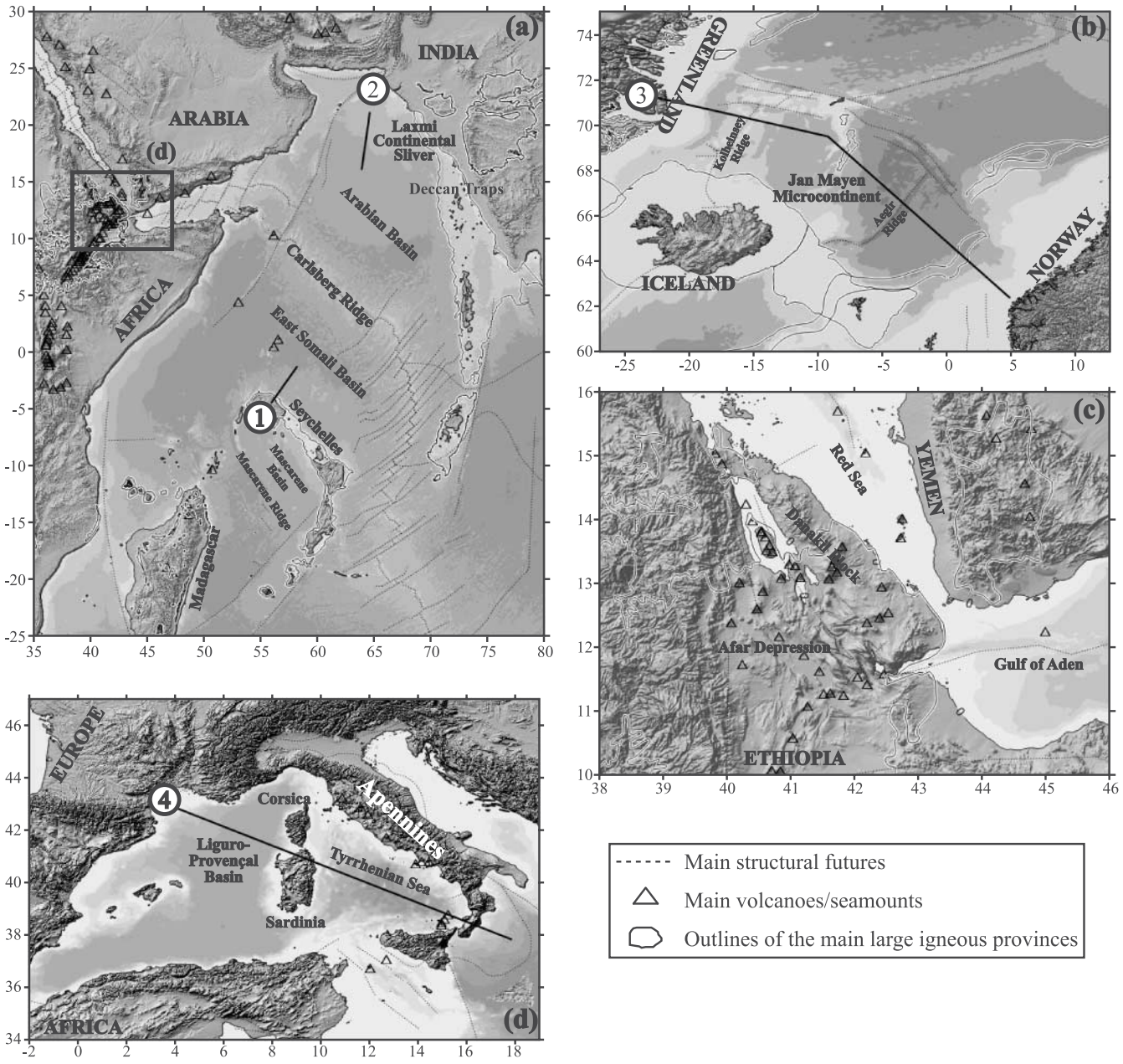

Fig. 1. Regional location and bathymetric maps of the microcontinents discussed in this paper. (**a**) Seychelles microcontinent and the Laxmi continental sliver in the India Ocean; (**b**) Jan Mayen microcontinent in the Norwegian–Greenland Sea; (**c**) Danakil proto-microcontinent in the Afar–Red Sea region; (**d**) Corsica–Sardinia continental block in the western Mediterranean Sea. The continuous black contours mark the extent of large igneous provinces after Coffin & Eldholm (1994). The bathymetry is from Sandwell & Smith (1997) and the topography from the Shuttle Radar Topography Mission datasets (http://srtm.usgs.gov/).

mantle) to an applied constant boundary velocity ($V_x = \pm 1$ cm a^{-1}) is examined, in which extension of the lithosphere is accommodated by thinning in the two regions that are weakened by the UPMBs emplaced at different times.

The force balance equation is solved, using the finite-element code tekton ver. 2.1 developed by Melosh & Raefsky (1980, 1981) and Melosh & Williams (1989). The viscoelastic–perfect plastic rheology model with temperature-dependent viscosity and the heat conduction model have been supplemented with the code (see also Yamasaki *et al*. 2008; Yamasaki & Gernigon 2009). Overlapping mechanical and thermal finite-element grids are used to sequentially solve the mechanical and heat equations.

The thermal equation is solved under the following boundary conditions. The temperature at the surface is held at 0 °C. At the left and right side boundaries of the model the horizontal heat flow is zero. Below a depth of 125 km, a temperature of 1350 °C is imposed as a constant temperature boundary condition, which implies that the thickness of the thermal lithosphere (a) is defined by the depth of the 1350 °C isotherm. The initial thermal structure is obtained by the steady-state solution. Advection of heat is incorporated by updating the finite-element grid at every time step with the displacement computed by the mechanical algorithm. Thermal parameter values are shown in Table 1.

The ductile deformation is modelled by means of a non-linear

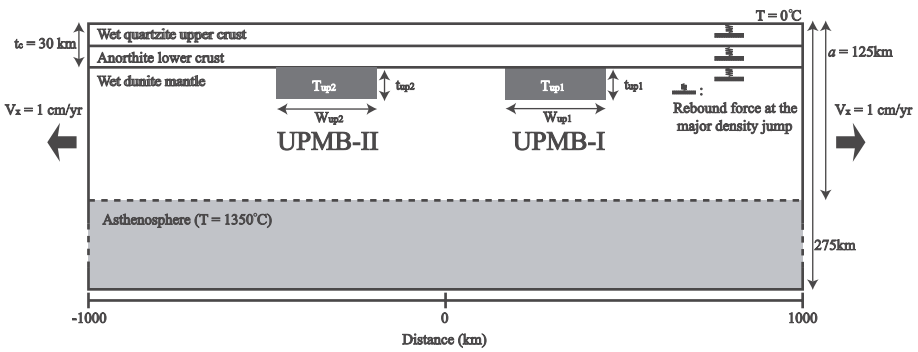

Fig. 2. Schematic illustration of the numerical model adopted in this study. The continental lithosphere has three compositional layers: wet quartzite upper crust, anorthite lower crust and wet dunite mantle. The initial thickness of the entire crust (t_c) is 30 km, in which the thicknesses of the upper and lower crust are 15 km. A constant horizontal boundary velocity ($V_x = \pm 1$ cm a^{-1}) is applied at the right and left side ends of the model. The Winkler restoring force is applied at the following major density interfaces so as to calculate the vertical surface movements: at the surface, the boundary between upper and lower crust, and at the Moho. The horizontal heat flow is set to zero at the right and left side boundaries of the model, and the temperature of the surface is fixed to be 0 °C. The temperature below the depth of 125 km is imposed to be 1350 °C as a constant temperature boundary condition, which indicates that the initial thickness of the thermal lithosphere (a) is defined by the depth of the 1350 °C isotherm. UPMB-I and -II with abnormally high temperature and mafic lower crustal composition are, respectively, characterized by W_{up1}, T_{up1} and t_{up1}, and W_{up2}, T_{up2} and t_{up2} at the point in time of its emplacement, where W_{up} is the width, t_{up} is the thickness and T_{up} is the temperature. It is assumed that the emplacement of UPMB-I and -II occurs at time $t = 0$ and Δt, respectively. The values of W_{up} and t_{up} adopted in this study are 50, 150 or 300 km and 5, 15 or 30 km, respectively. The values of T_{up1} are 600, 800 and 1000 °C, but T_{up2} is assumed to have a unique value of 1000 °C.

Maxwell viscoelastic rheology. The effective viscosity (η) prescribed by power-law creep is written in the form

$$\eta = (1/2A^*)J_{2D}^{(1-n)/2} \exp(Q/RT) \quad (1)$$

where A^* is a material constant, Q is the activation energy, n is the stress exponent, R is the universal gas constant and T is the absolute temperature. On the other hand, an elastic–perfect plastic rheology model is adopted for the brittle behaviour of rocks. The yielding is controlled by the Von Mises criterion:

$$J_{2D} - \sigma_y^2/3 = 0 \quad (2)$$

where σ_y is the yield stress. In this study, σ_y is assumed to follow the depth-dependent brittle stress:

$$\sigma_y = \zeta(1 - \upsilon^*)z \quad (3)$$

where z is the depth in km, ζ is a constant (24 MPa km^{-1}) and υ^* (0.4) is the density ratio of pore water to rock matrix. Rheological parameters used in this study are summarized in Table 1.

The UPMB is introduced as a simplified material unit with anomalously high temperature and a mafic lower crustal composition (see also Table 1). Each UPMB is described by the following three parameters: width (W_{up}), thickness (t_{up}) and temperature (T_{up}). Configuration of the two UPMBs (UPMB-I and UPMB-II) is, respectively, characterized by T_{up1}, W_{up1}, t_{up1} and T_{up2}, W_{up2}, t_{up2} at the point in time of the emplacement (Fig. 2). The first deformation localization is obtained by the emplacement of UPMB-I at time $t = 0$, with the centre of the body located at $x = 200$ km. Then, we artificially assume the emplacement of UPMB-II at $t = \Delta t$ to possibly trigger the redistribution of deformation, with the centre of the second body located at $x = -200$ km.

For simplification, it is assumed that the UPMB is emplaced instantaneously without taking into account the nature of the melt generation and its upward migration (e.g. Frey *et al*. 1998; Callot *et al*. 2001; Yamasaki & Gernigon 2009). As indicated by many studies (e.g. Burke & Dewey 1973; Sengör & Burke 1978; Griffiths & Campbell 1991; Menzies *et al*. 2002; Al-Kindi *et al*. 2003; Courtillot & Renne 2003; Buck 2006), the magmatic event could occur prior to the rifting process. Therefore, the UPMB could work as the local rheological heterogeneity where rifting can be initiated.

The ascent of the asthenosphere into the lithosphere would be required to generate the melts, which may imply that the thermal thinning of the lithosphere prior to the emplacement of the UPMB could also work as a weak zone to induce deformation localization (e.g. Gac & Geoffroy 2009). However, Yamasaki & Gernigon (2009) previously indicated that the reduction of the total lithospheric strength is more significant and efficient if the shallower (colder) part of the lithosphere is weakened. The temperature in the deepest region of the lithosphere is originally so high that it is difficult for any asthenosphere-related weakening to be perceptible.

Figure 3a shows the temperature profile in the lithosphere, in which the temperature at depths greater than D_{as} is artificially imposed to be 1350 °C by presuming that the asthenosphere penetrates to a depth of D_{as} in a geologically short period. Using these temperature profiles, the stress envelopes in the lithosphere are drawn in Figure 3b, where the strain rate is assumed to be 10^{-15} (s^{-1}). It is shown that a significant difference is not perceptible between models if D_{as} is deeper than 50 km. The difference in the integrated total strength of the lithosphere (ΔS) from the model with no asthenosphere penetration ($D_{as} =$ 125 km) is shown in Figure 3c. ΔS becomes greater as D_{as} becomes smaller (i.e. as the asthenosphere penetrates to a shallower level in the lithosphere). However, ΔS is restricted to be less than 0.5 TN m^{-1} as long as D_{as} is greater than 60 km. Thus, even if the generation of the melts requires the thermal thinning of the lithosphere, its thinning does not seem to work as a principal weak zone to localize the deformation as long as the ascent of the asthenosphere is restricted to a depth greater than c. 60 km.

Table 1. Model parameter values used in this study

Symbol	Meaning	Value
E	Young's modulus	1.5×10^{11} Pa
ν	Poisson's ratio	0.25
ζ	Depth dependence of brittle failure	24.0 MPa km^{-1}
υ*	Density ratio of pore water to rock	0.4
C_p	Specific heat	1050 J kg^{-1} K^{-1}
R	Universal gas constant	8.314 J mol^{-1} K^{-1}
T_a	Potential temperature of the asthenosphere	1350 °C
T_s	Temperature at the surface	0 °C
ρ_{uc}	Density of the upper crust	2800 kg m^{-3}
ρ_{lc}	Density of the lower crust	2900 kg m^{-3}
ρ_m	Density of the mantle	3300 kg m^{-3}
H_{uc}	Heat production in the upper crust	1.37 μW m^{-3}
H_{lc}	Heat production in the lower crust	0.45 μW m^{-3}
H_m	Heat production in the mantle	0.02 μW m^{-3}
K_{uc}	Thermal conductivity of the upper crust	2.56 W m^{-1} K^{-1}
K_{lc}	Thermal conductivity of the lower crust	2.60 W m^{-1} K^{-1}
K_m	Thermal conductivity of the mantle	3.20 W m^{-1} K^{-1}
Flow law parameters of power law creep		
Wet quartzite: Koch et al. (1989)		
A^*_{ucw}	Pre-exponent	1.10000×10^{-21} Pa^{-n} s^{-1}
n_{ucw}	Power	2.61
Q_{ucw}	Activation energy	145 kJ mol^{-1}
Anorthite: Shelton & Tullis (1981)		
A^*_{lc}	Pre-exponent	5.60000×10^{-23} Pa^{-n} s^{-1}
n_{lc}	Power	3.20
Q_{lc}	Activation energy	238 kJ mol^{-1}
Wet Aheim dunite: Chopra & Paterson (1984)		
A^*_{mw}	Pre-exponent	5.4954×10^{-25} Pa^{-n} s^{-1}
n_{mw}	Power	4.48
Q_{mw}	Activation energy	498 kJ mol^{-1}
Mafic granulite: Wilks & Carter (1990) and Ranalli (1995)		
A^*_{upmb}	Pre-exponent	8.8334×10^{-22} Pa^{-n} s^{-1}
n_{upmb}	Power	4.2
Q_{upmb}	Activation energy	445 kJ mol^{-1}

For the continental lithosphere, because of its great thickness, it takes a long time (more than a few tens of million years) to thermally influence the shallower level of the lithosphere by either the conductive or convective heat transfer (e.g. Spohn & Schubert 1982; Yuen & Fleitout 1985). Contrarily, a large amount of melt can be generated in the early stage of the thermal thinning (e.g. Harry & Leeman 1995; van Wijk *et al*. 2001), and the upward migration of the produced melts must be very quick as any remnants of the melts are not clearly detected by geophysical observation (e.g. Reid & Jackson 1981; Sparks & Parmentier 1991). Melt stagnation is, however, still possible in the uppermost mantle (Müntener & Manatschal 2006). Therefore, the emplacement of the UPMB into the shallower level in the lithosphere is likely to be considered as a principal mechanism of deformation redistribution, especially in an early stage of the lithospheric thinning.

As indicated by geological and geophysical considerations (e.g. Mjelde *et al*. 2005; White & Smith 2009; Yamasaki & Gernigon 2009), the thickness and width of the UPMB would have some variations, depending on the amount of melt production. W_{up} and t_{up} are, therefore, assumed to have the values of 50, 150 or 300 km and 5, 15 or 30 km, respectively. Three values of the temperature for UPMB-I (T_{up1}) are adopted; 600, 800 and 1000 °C. This temperature should be dependent on the time when the extension is initiated after the emplacement of UPMB-I. On the other hand, UPMB-II must have a high temperature because its emplacement occurs during the extensional process. Therefore, T_{up2} is assumed to have a unique value of 1000 °C in this study. The time between the emplacement of the two UPMB (Δt) is taken to be 1.0, 2.5, 5.0, 7.5, 10.0, 12.5 or 15.0 Ma.

In practice, the rheological heterogeneity does not always have to be caused by the emplacement of a UPMB. There are many other origins of rheological heterogeneity prior to and during extension (e.g. Fernàndez & Ranalli 1997, and references therein; Pérez-Gussinyé & Reston 2001; Péron-Pinvidic & Manatschal 2008; Corti 2009). Therefore, the configuration of the UPMB in our study could be implicitly regarded as an indicator of any rheological heterogeneity, whatever the source of the deformation localization. The UPMB particularly considered in this study is no more than one possible origin of the heterogeneity.

Results

Figure 4a shows the deformed grids and temperature structure of the model at the time $t = 12$ Ma, where $T_{up1} = 600$ °C, $W_{up1} = 150$ km, $t_{up1} = 5$ km, $W_{up2} = 150$ km, $t_{up2} = 15$ km, and $\Delta t = 5.0$ Ma. It is clearly shown that the deformation localization is completely shifted to the region where UPMB-II is emplaced.

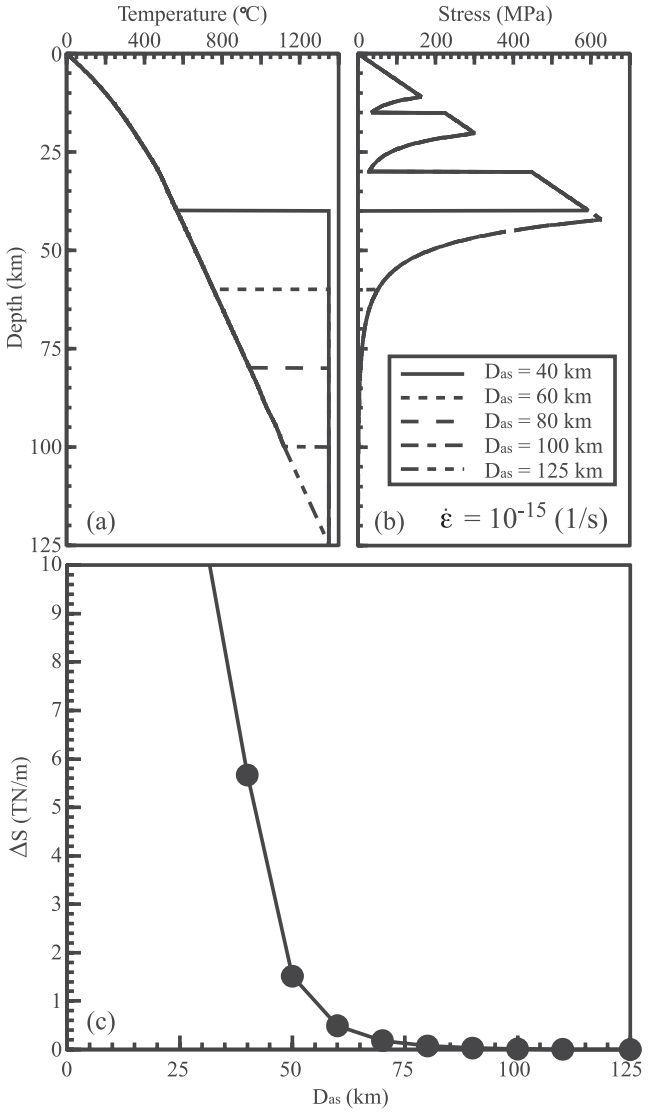

Fig. 3. (**a**) Temperature profile for a different penetration depth of the asthenosphere (D_{as} = 125, 100, 80, 60 and 40 km). (**b**) Stress envelope based on the temperature profile shown in (**a**), where applied strain rate is 10^{-15} (s^{-1}). (**c**) Difference in the total strength of the lithosphere from the model with D_{as} = 125 km.

Figure 4b shows the temporal profile of the total stretching factor of the lithosphere (β_t). Before UPMB-II is emplaced, the applied extension of the lithosphere is accommodated only by thinning of the region where UPMB-I is present (domain-I). However, once UPMB-II is emplaced, the extension becomes accommodated by thinning of the region where UPMB-II is emplaced (domain-II), and the thinning in domain-I ends. We define this kind of model behaviour as 'a shift-completed mode'.

Figure 5 shows the results of the model, where $T_{up1} = 600$ °C, $W_{up1} = 50$ km, $t_{up1} = 5$ km, $W_{up2} = 50$ km, $t_{up2} = 15$ km, and $\Delta t = 7.5$ Ma. As also shown in Figure 4, extension of the lithosphere is accommodated only by thinning of domain-I prior to the emplacement of UPMB-II. However, in this model, the emplacement of UPMB-II results in the lithospheric extension being accommodated by thinning in both domains-I and -II. Deformation localization is clearly redistributed, but not completely shifted. In this study, this behaviour is defined as 'a transition mode'.

Figure 6 shows the results of the model, where $T_{up1} = 600$ °C, $W_{up1} = 50$ km, $t_{up1} = 5$ km, $W_{up2} = 50$ km, $t_{up2} = 15$ km, and $\Delta t = 10.0$ Ma. In this model, even though UPMB-II is emplaced, the total stretching factor in domain-II does not increase significantly and the extension is accommodated only by thinning of domain-I. The thermal anomaly caused by the emplacement of UPMB-II can be seen in the figure, but its weakening effect does not allow the deformation to redistribute. Domain-I has become so weak that UPMB-II cannot initiate thinning in domain-II. In this study, such model behaviour is defined as 'a shift-failed mode'.

The three modes of deformation redistribution are summarized in Figure 7. The horizontal axis indicates the averaged strain rate ($\dot{\varepsilon}_{av}$) in domain-I in the period Δt. Even if the applied boundary velocity is unique, a variety of initial strain rates is obtained, depending on the configuration of UPMB-I (Yamasaki & Gernigon 2009). Additionally, the strain rate can change through time even for a given constant boundary velocity, because rheological features in the deforming region change in accordance with lithospheric thinning and thermal relaxation. Therefore, we adopt an averaged strain rate ($\dot{\varepsilon}_{av}$), instead of the initial strain rate. The vertical axis indicates the total stretching factor (β_t) in domain-I at the time when UPMB-II is emplaced.

It could be expected that the boundaries between the three redistribution modes are principally controlled by $\dot{\varepsilon}_{av}$, in which a smaller β_t is required for models with higher $\dot{\varepsilon}_{av}$ to exhibit the redistribution modes in which shifting of deformation occurs. However, as can be seen in Figure 7, the boundaries are actually not explained only in terms of $\dot{\varepsilon}_{av}$.

The different configurations of the UPMBs are not distinguished in Figure 7, but we have confirmed the following general sensitivities of the parameters. Models with greater t_{up1} and T_{up1} and smaller W_{up1} require an earlier emplacement of UPMB-II to facilitate the shift-completed or transition modes. This is explained by noting that models with such UPMB-I configuration predict a relatively high strain rate in the first deformed region (Yamasaki & Gernigon 2009) and, accordingly, a relatively large thermal weakening (i.e. thinning factor) is obtained for a given time.

Models with smaller W_{up2}, T_{up2} and t_{up2} do not favour the modes that shift deformation regardless of the parameters describing the UPMB-I. This indicates that the redistribution of the deformation localization is also strongly controlled by the UPMB-II configuration. However, models with $T_{up1} \geqslant 800$ °C and $t_{up1} \geqslant 15$ km do not allow the deformation to redistribute for any configuration of UPMB-II. It is self-evident that the redistribution is hardly obtained by a UPMB-II that has the same configuration as UPMB-I when the deformation in domain-I shows that the weakening caused by the increase in geothermal gradient exceeds the strengthening caused by the crustal thinning and thermal diffusion.

It is also important to note that once the total stretching factor of the lithosphere in the first deformed region exceeds *c*. 2.25, the redistribution of the deformation can no longer be obtained, regardless of the configurations of UPMB-I and -II (see Fig. 7).

Discussion

General model behaviour

We have demonstrated that the deformation can be redistributed into a different region if rheological heterogeneity is introduced

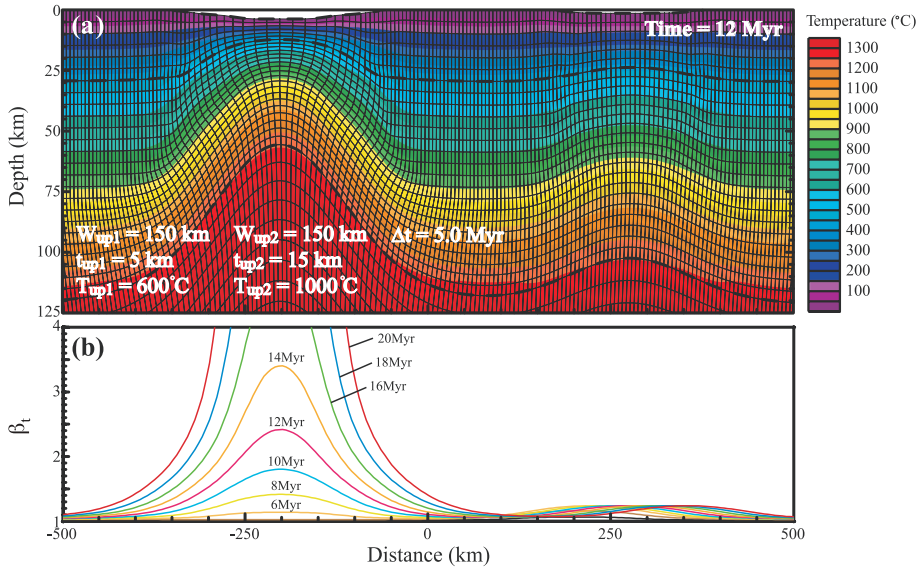

Fig. 4. (**a**) Deformed grids and temperature structure of the model at the time $t = 12$ Ma. (**b**) Temporal evolution of the total stretching factor of the lithosphere. Parameter values of the UPMBs are $W_{up1} = 150$ km, $t_{up1} = 5$ km, $T_{up1} = 600$ °C, $W_{up2} = 150$ km, $t_{up2} = 15$ km, $T_{up2} = 1000$ °C and $\Delta t = 5$ Ma.

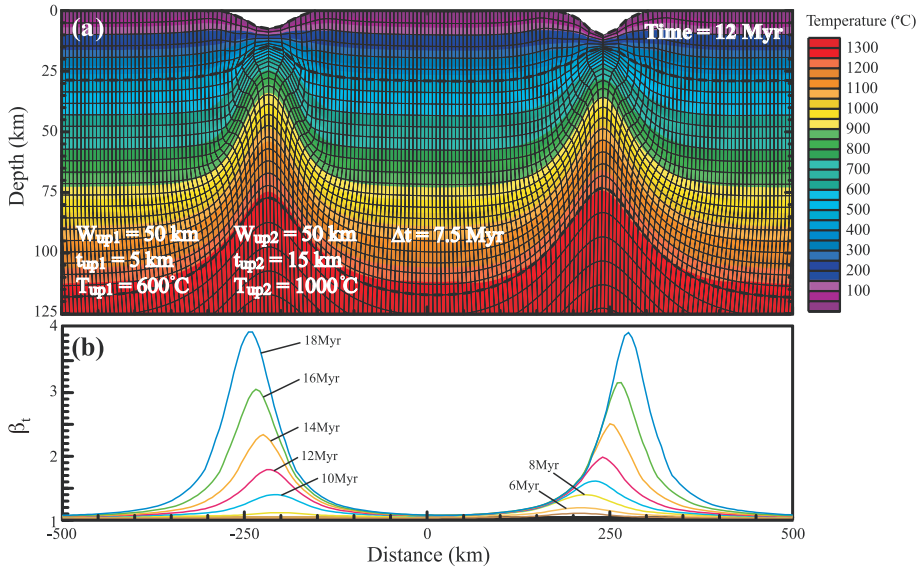

Fig. 5. (**a**) Deformed grids and temperature structure of the model at the time $t = 12$ Ma. (**b**) Temporal evolution of the total stretching factor of the lithosphere. Parameter values of the UPMBs are $W_{up1} = 50$ km, $t_{up1} = 5$ km, $T_{up1} = 600$ °C, $W_{up2} = 50$ km, $t_{up2} = 15$ km, $T_{up2} = 1000$ °C and $\Delta t = 7.5$ Ma.

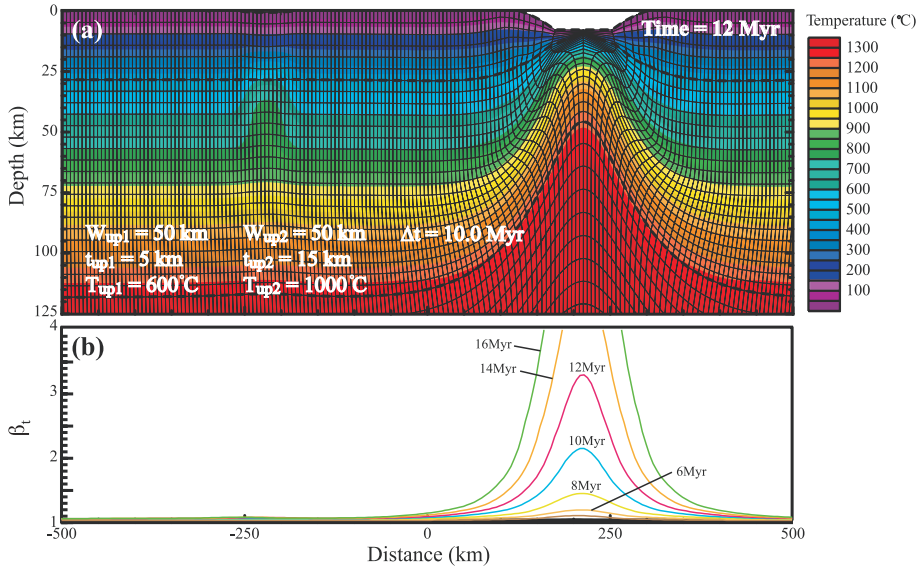

Fig. 6. (**a**) Deformed grids and temperature structure of the model at the time $t = 12$ Ma. (**b**) Temporal evolution of the total stretching factor of the lithosphere. Parameter values of the UPMBs are $W_{up1} = 50$ km, $t_{up1} = 5$ km, $T_{up1} = 600$ °C, $W_{up2} = 50$ km, $t_{up2} = 15$ km, $T_{up2} = 1000$ °C and $\Delta t = 10$ Ma.

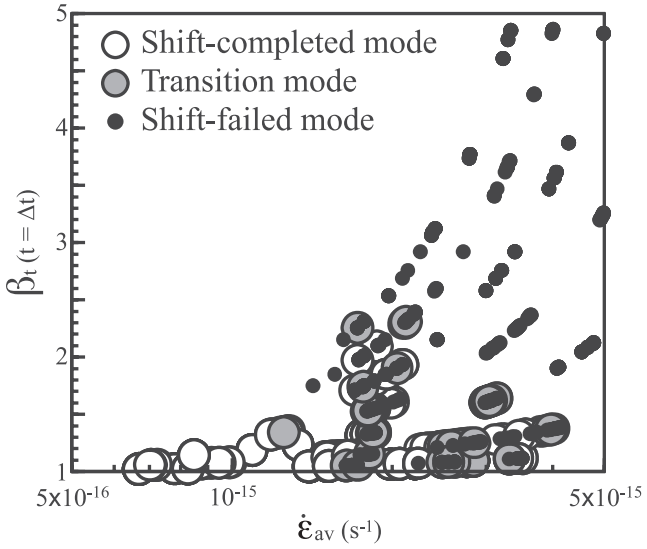

Fig. 7. Distribution of the three modes of the deformation redistribution as functions of the averaged strain rate ($\dot{\varepsilon}_{av}$) and the total stretching factor of the lithosphere (β_t) at the time when the UPMB-II is emplaced.

by the UPMB's emplacement during the extensional process. It has been shown that three modes of the deformation redistribution can be present: (1) the shift-completed mode where the deformation localization is completely shifted into the new region; (2) the transition mode where the localization takes place at the two regions; (3) the shift-failed mode where the deformation localization is not shifted at all. The modes are dependent both on the initial rheological heterogeneity in the first deformed region and on the configuration of the UPMB emplaced during extension.

The change in the strength of the lithosphere during extension has been usually discussed in terms of the competition between the weakening caused by the increase in the geothermal gradient and the strengthening caused by the crustal thinning and thermal relaxation, in which it has been emphasized that the strain rate plays an important role (e.g. England 1983; Takeshita & Yamaji 1990). However, as shown in the present study, it is difficult to prescribe the boundaries between the three redistribution modes only in terms of the strain rate-controlled thermal relaxation in the first deformed region (see Fig. 7). This can be intuitively understood by noting that if substantial weakening is obtained by the thermal and compositional anomalies of UPMB-II the redistribution of the deformation is no longer controlled by the thermal process in the first deformed region.

As described by Yamasaki & Gernigon (2009), the initial strain rate in the first deformed region depends on the UPMB-I configuration and increases when there is a greater strength contrast between the weakened and non-weakened regions. If this contrast is insignificant, an applied extension is accommodated not only by thinning of the weakened region but also by thinning of the non-weakened region (Yamasaki & Gernigon 2009). That is, models with small t_{up1} and small T_{up1} would result in a slow initial strain rate, and an available thermal anomaly in the first deformed region is also so small that only the shift-completed mode can be predicted, which explains the results of the models with the averaged strain rate ($\dot{\varepsilon}_{av}$) $< c.\ 10^{-15}$ s^{-1} (see also Fig. 7). If the later emplacement of UPMB-II ($\Delta t > 15$ Ma) is applied in such a range of the UPMB-I configurations and the weakening brought about by UPMB-II does not exceed the strengthening by thermal relaxation in the first deformed region, the redistribution mode could possibly be prescribed by $\dot{\varepsilon}_{av}$. However, as has been discussed in many previous studies, the deformation redistribution is mainly controlled by thermal relaxation, and the role of the UPMB's emplacement declines to only a collateral effect to promote redistribution.

On the other hand, if the weakening brought about by UPMB-I is large enough to accommodate the lithosphere extension almost entirely by the thinning of the weakened region, then the initial strain rate for a given W_{up1} is principally controlled by the applied boundary velocity. In the case where the boundary velocity is large enough that the thermal relaxation during extension is a minor effect, the question of whether or not the deformation localization is redistributed depends on the configuration of UPMB-II, and accordingly the modes of the deformation redistribution are not solely prescribed by the strain rate in the first deformed region. In situations where the deformation redistribution is primarily controlled by UPMB-II, a greater amount of thermal and compositional anomaly (i.e. models with greater W_{up2}, T_{up2} and t_{up2}) more efficiently redistributes the deformation. However, the interpretation described above concerns only the case where UPMB-II is emplaced before the first deformed region exceeds the critical stretching factor.

It should be noted that the value of the critical stretching factor (*c*. 2.25) shown in this study was determined for a given boundary condition (i.e. $t_c = 30$ km, $a = 125$ km and $V_x = \pm 1$ cm a^{-1}), and it could possibly change for different lithosphere structure and boundary velocity. However, it is not the aim of the present study to evaluate the critical stretching factor for various boundary conditions, and the most important point that we should emphasize is the fact that there exists the critical stretching factor for the redistribution modes, whatever its value is.

In practice, it would be difficult for any geological evidence to clearly reveal the stretching factor in the first deformed region at the time when a UPMB is emplaced in a different region. However, the geological or geophysical field data can provide, at least to some extent, the time when sea-floor spreading is established, and it can be inferred from our model results that deformation redistribution is difficult to trigger after the onset of spreading in the first deformed region. Therefore, as a first-order approximation, we can discuss the observed deformation migration in terms of our redistribution modes (i.e. the shift-completed and transition modes) provided that the emplacement of a UPMB occurs significantly before the onset of spreading in the first deformed region.

Implications for microcontinent formation

Here, we particularly attempt to discuss microcontinent formation in relation to the numerical model behaviour in this study, by taking up the examples from the Indian Ocean, the Norwegian–Greenland Sea, the Red Sea–Afar region and the western Mediterranean (see Fig. 1).

The formation of a microcontinent, a continental block isolated between two spreading system, may possibly be interpreted as a product of the deformation redistribution induced by a UPMB. It has been interpreted by noting that the termination of sea-floor spreading followed by the establishment of a new spreading system in a different place causes a microcontinent to be segregated. That is, microcontinent formation is always accompanied by the cessation of the earlier spreading. This alludes to a simple application of the shift-completed mode as an

explanation for the sudden redistribution of the deformation localization, as has previously been considered for microcontinent formation. However, our numerical experiment has shown that it is difficult to redistribute the deformation localization if the first deformed region exceeds the critical stretching factor (see Fig. 7). Therefore, the shift-completed mode cannot be applied, because the total stretching factor of the lithosphere would be largely beyond this critical value during the onset of continental break-up.

For that reason, it is only possible to apply the transition mode to the formation of microcontinent. In this mechanism, the deformation proceeds in two regions, but the timing when the rifting process leads to the break-up is different between the two regions. The deformation may eventually become completely concentrated into either deforming domain, depending on the particular magmatic characteristics of the two regions, as we have shown (e.g. the configuration of UMPB-II), which may lead to the ending of the earlier spreading.

The microcontinent formations in the Indian Ocean (i.e. the Seychelles microcontinent and the Laxmi continental sliver) may be explained by the framework of the transition mode. The Seychelles microcontinent and the Laxmi continental sliver are located between the three spreading systems (Figs 1a and 8) the Mascarene Ridge, the Carlsberg Ridge and the spreading in the Gop Basin, which were established at *c*. 84 Ma, *c*. 64 Ma and *c*. 69 Ma, respectively (McKenzie & Sclater 1971; Norton & Sclater 1979; Masson 1984; Bhattacharya *et al*. 1994; Talwani & Reif 1998; Todal & Edholm 1998; Bernard & Munschy 2000; Collier *et al*. 2008, 2009; Yatheesh *et al*. 2009). The tilted fault blocks in both the northeastern margin of the Seychelles and the western India–Pakistan margin have been interpreted as a synrift structure during the late Cretaceous (Plummer & Bellé 1995; Subrahmanya 1998; Carmichael *et al*. 2009). This clearly supports that the rifting in the Arabia–East Somali Basin had already been initiated while the Gop Basin was still in the rifting phase (before the spreading phase).

The pre-Deccan volcanic event also occurred in the late Cretaceous (Collier *et al*. 2008), which is possibly consistent with the tilted synrift blocks and the volcanic event occurring synchronously. A widespread high-velocity body is present beneath the region (see Fig. 8), which may imply that it is difficult to obtain any deformation localization. However, the deformation redistribution into a particular region can be explained by considering the heterogeneity of the UPMB thickness. Thus, the formation of the Laxmi continental sliver can be explained by applying the transition mode, in which the emplacement of the UPMB brought about by the pre-Deccan volcanic event induced the redistribution of the deformation between the Gop Basin and the Arabia–East Somali Basin.

On the other hand, because the spreading in the Mascarene Basin was initiated prior to the rifting initiation in the Arabia–East Somali Basin, even the transition mode is not applicable for the Seychelles microcontinent. It may be interpreted that there was no deformation redistribution between the Mascarene Basin and the Arabia–East Somali Basin, and the isolation of the Seychelles microcontinent is only an incidental product as the result of the deformation redistribution between the Gop Basin and the Arabia–East Somali Basin.

We also attempt to apply the transition mode for the formation of the Jan Mayen microcontinent located between the following two spreading ridges in the Norwegian–Greenland Sea, the Aegir Ridge and the Kolbeinsey Ridge, where the spreading was established in the Early Eocene and in the Late Oligocene, respectively (Gudlaugsson *et al*. 1988; Kuvaas & Kodaia 1997; Skogseid *et al*. 2000; Mjelde *et al*. 2008; see Figs 1b and 9). The study of a buried rift in the conjugate Greenland margin revealed that the rifting could have already been active during the Cretaceous to Palaeocene (e.g. Larsen 1984; Hamann *et al*. 2005), implying that the rifting initiation itself could be earlier than the onset of the spreading along the Aegir Ridge, which is also supported by the plate reconstruction model of Gaina *et al*. (2009). In addition, the magmatic event in the Palaeocene recorded in the east Greenland margin (Meyer *et al*. 2007; Tegner *et al*. 2008) does not contradict the rifting process occurring simultaneously with the emplacement of a UPMB. Thus, it is possible to explain the Jan Mayen microcontinent formation in terms of the transition mode.

In regard to the application of the transition mode to the formation of microcontinents, the thinning in the second deformed region has to continue even after the first deformed region reaches break-up; this is probably possible unless the strength difference between the two domains becomes significantly larger. Indeed, such a transient process of transition mode is currently observed in the Afar–Red Sea region, where the rifting process has still been active in the Afar depression even after the onset of the spreading in the Red Sea (Fig. 1c).

The Danakil Block is a proto-microcontinent located between the Red Sea and the Afar depression (Manighetti *et al*. 1998;

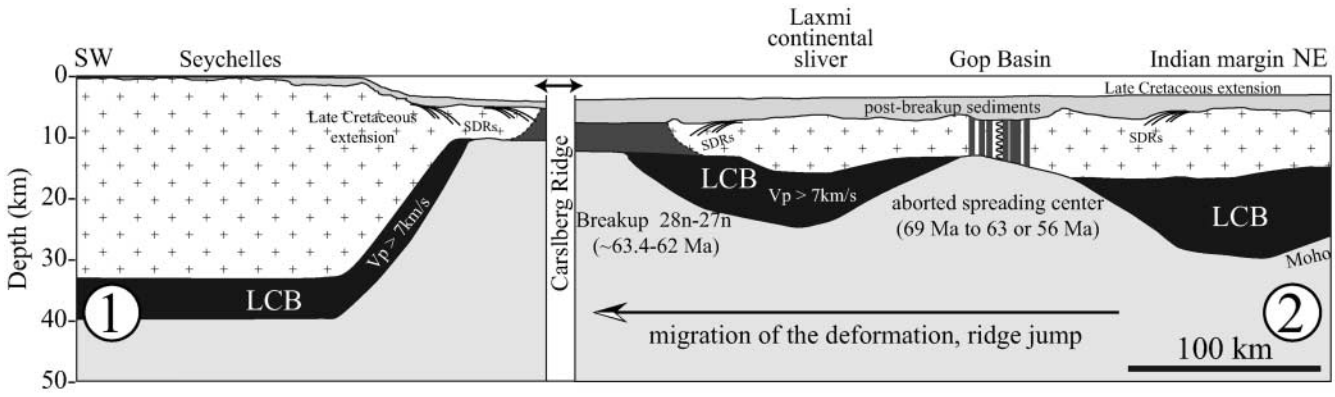

Fig. 8. Regional transect across the conjugate Seychelles–Western India–Pakistan margin (modified after Collier *et al*. 2009). Location of the transect is shown in Figure 1a. The northern part of the Western India–Pakistan margin is characterized by the presence of the Laxmi continental sliver, located between the Arabian Basin and the Gop Basin. LCB, high-velocity lower crustal body; SDRs, seaward-dipping reflectors.

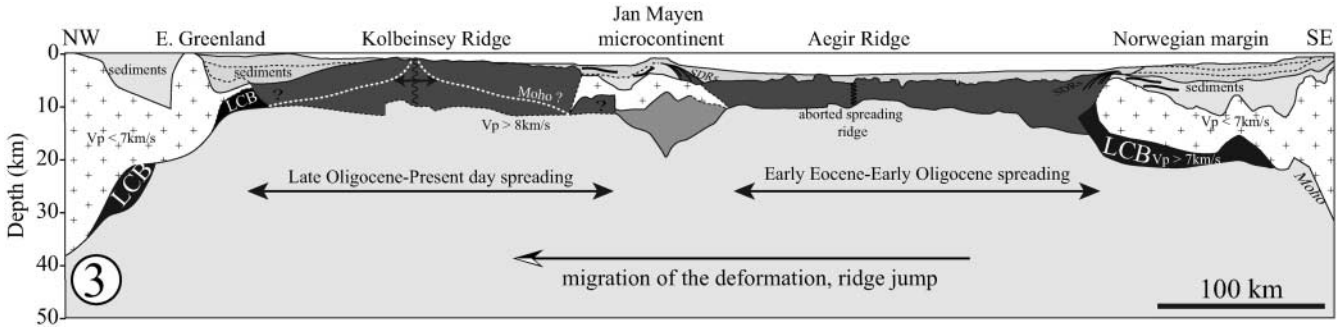

Fig. 9. Regional transect between Greenland and Norway across the Jan Mayen microcontinent (modified after Mjelde *et al*. 2008). Location of the transect is shown in Figure 1b. The Jan Mayen microcontinent is located between the two spreading systems, the Kolbeinsey Ridge and the Aegir Ridge.

Eagles *et al*. 2002; Beyene & Abdelsalam 2005; Garfunkel & Beyth 2006; Le Gall *et al*. 2010). The rifting process in the Red Sea and the Afar depression started around 31–28 Ma, shortly after major volcanism in Ethiopia and Yemen (Garfunkel & Beyth 2006), in which the extensional tectonics in the Afar depression had been activated significantly before the onset of sea-floor spreading in the Red Sea (Beyene & Abdelsallam 2005; Garfunkel & Beyth 2006). Seismic studies have also observed that igneous material was added to form a highly attenuated transitional crust beneath the Afar depression (Makris & Ginzburg 1987; Dugda *et al*. 2005). The formation of the Danakil proto-microcontinent can therefore be regarded as a good modern analogue showing the transient behaviour of the transition mode in which the magmatic activity triggered the deformation redistribution.

The formation of the Corsica–Sardinia block in the western Mediterranean Sea (see Figs 1d and 10) may also be described in the same way. The opening of the Liguro-Provençal Basin, followed by that of the Tyrrhenian Sea, had isolated the Corsica–Sardinia block (e.g. Doglioni *et al*. 1997; Lonergan & White 1997; Gueguen *et al*. 1998; Faccenna *et al*. 2001). However, the ages of the oldest synrift deposits in the northern and southern Tyrrhenian Sea are early and late Miocene, respectively (e.g. Kasten *et al*. 1988; Jolivet *et al*. 1998; Mauffret & Contrucci 1999), which indicates that rifting in the Tyrrhenian Sea was initiated after the Liguro-Provençal Basin had reached the spreading phase at *c*. 22–23 Ma (e.g. Faccenna *et al*. 2001; Gattacceca *et al*. 2007). Therefore, the transition mode cannot be employed for the microcontinent formation in this region. The Corsica–Sardinia block may be interpreted to suggest that, during the temporal intermission of the extension between 15 and 10 Ma (e.g. Faccenna *et al*. 2001), the increase in the lithospheric strength beneath the Liguro-Provençal Basin significantly progressed in accordance with the thermal relaxation, and the subsequent deformation was concentrated only into the unextended Tyrrhenian Sea. It is also noted that there is no clear evidence of a UPMB beneath the region, which may emphasize the importance of the UPMB emplacement for applying the transition mode.

Concluding remarks

In this study, we have examined the redistribution of deformation triggered by the emplacement of a UPMB. It has been shown that there are three modes of deformation redistribution (the shift-completed mode, the transition mode and the shift-failed mode) depending on the initial rheological heterogeneity developed in the first deformed region and on the configuration of the UPMB's emplacement during extension. However, it is difficult to obtain the redistribution of the deformation if its emplacement occurs after the total stretching factor of the lithosphere in the first deformed region exceeds the critical value.

Based on the numerical model behaviour in this study, we have discussed the microcontinent formations observed in the Indian Ocean, the Norwegian–Greenland Sea, the Afar–Red Sea region and the western Mediterranean Sea, proposing the transition mode as a new framework for the interpretation. It has been shown that the (proto-)microcontinent formations in the Indian

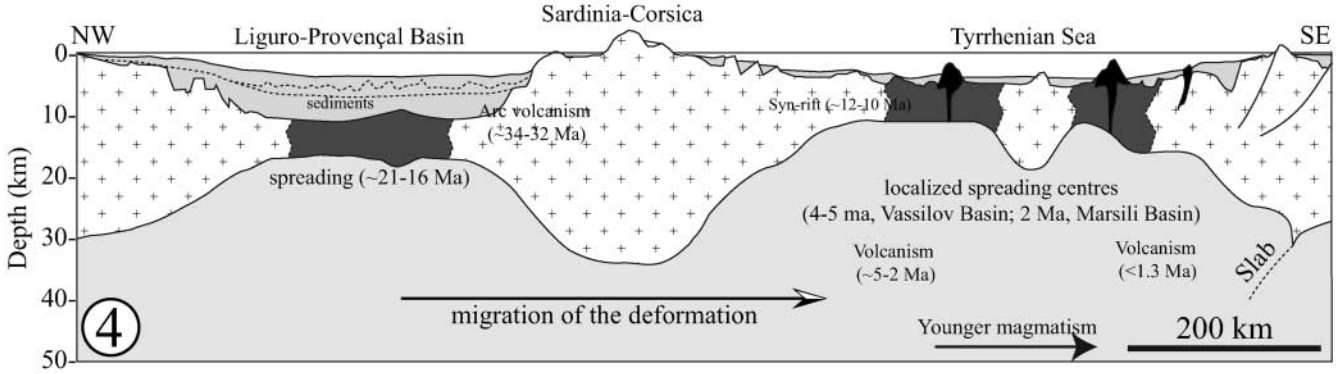

Fig. 10. Regional transect across the West Mediterranean Sea (modified after Faccenna *et al*. 2001). Location of the transect is shown in Figure 1d. The Corsica–Sardinia block is interpreted as a microcontinent that has been insulated between the two spreading systems including the Liguro-Provençal Basin and the Tyrrhenian Sea.

Sea, the Norwegian–Greenland Sea and the Afar–Red Sea region can be explained by applying the transition mode, in which another rifting process in a different region is initiated significantly before the onset of the sea-floor spreading in the first deformed region. However, it has also been recognized that it is difficult for the transition mode to explain the formation of the Corsica–Sardinia continental block in the western Mediterranean. Therefore, the transition mode is not always applicable for any microcontinent, especially for the case where the presence of a UPMB is not clearly observed. However, it allows us to categorize the style of microcontinent formation and aids in our understanding of its mechanism.

Further investigations are also required to elucidate what effectively controls the emplacement of the UPMB. Its origin may be discussed in relation to the dynamics of the asthenosphere beneath continents (e.g. White & McKenzie 1989; Farnetani & Richards 1994; King & Anderson 1998). Although the nature of the UPMB's emplacement is still difficult to understand, the critical stretching factor for the deformation migration may offer an important constraint on the timing and the deep origin of the UPMB.

C. Gaina and G. Péron-Pinvidic are acknowledged for stimulating discussion about the Jan Mayen microcontinent. We are grateful to J. Mound for carefully reading the manuscript and valuable suggestions. We would like to thank J. Skogseid for valuable suggestions. Constructive and critical reviews by G. Corti and an anonymous reviewer improved the manuscript. T.Y. thanks K. Wang for sharing the finite-element code tekton ver. 2.1 and for allowing modification of the code. J. Melosh and A. Raefsky are also acknowledged as the authors of the original code. The calculations in this study were carried out on the computer facility at the Dublin Institute for Advanced Studies. This study is supported by the NGU–Statoil project: Breakup and microcontinent formation: investigation of the Jan Mayen and conjugate margins system.

References

Al-Kindi, S., White, N., Sinha, M., England, R. & Tiley, R. 2003. Crustal trace of a hot convective sheet. *Geology*, **31**, 207–210.

Bernard, A. & Munschy, M. 2000. Were the Mascarene and Laxmi Basins (western Indian Ocean) formed at the same spreading centre? *Comptes Rendus de l'Académie des Sciences, Série IIA*, **330**, 777–783.

Beyene, A. & Abdelsalam, M.G. 2005. Tectonics of the Afar depression: A review and synthesis. *Journal of African Earth Sciences*, **41**, 41–59.

Bhattacharya, G.C., Chaubey, A.K., Murty, G.P.S., Srinivas, K., Sarma, K., Subrahmanyam, V. & Krishna, K.S. 1994. Evidence for sea-floor spreading in the Laxmi Basin, northeastern Arabian Sea. *Earth and Planetary Science Letters*, **125**, 211–220.

Braun, J. 1992. Post extensional mantle healing and episodic extension in the Canning Basin. *Journal of Geophysical Research: Solid Earth*, **97**, 8927–8936.

Buck, W.R. 2006. The role of magma in the development of the Afro-Arabian Rift System. *In:* Yirgu, G., Ebinger, C.J. & Maguire, P.K.H. (eds) *The Afar Volcanic Province within the East African Rift System*. Geological Society, London, Special Publications, **259**, 43–54.

Burke, K. & Dewey, J.F. 1973. Plume-generated triple junctions: Key indicators in applying plate tectonics to old rocks. *Journal of Geology*, **81**, 406–433.

Callot, J.P., Grigne, C., Geoffroy, L. & Brun, J.P. 2001. Development of volcanic passive margins: Two-dimensional laboratory models. *Tectonics*, **20**, 148–159.

Carmichael, S.M., Akhter, S., Bennett, J.K., *et al.* 2009. Geology and hydrocarbon potential of the offshore Indus Basin, Pakistan. *Petroleum Geoscience*, **15**, 107–116.

Chopra, P.N. & Paterson, M.S. 1984. The role of water in the deformation of dunite. *Journal of Geophysical Research: Solid Earth*, **89**, 7861–7876.

Coffin, M. F. & Eldholm, O. 1994. Large igneous provinces—crustal structure, dimensions, and external consequences. *Reviews of Geophysics*, **32**, 1–36.

Collier, J.S., Sansom, V., Ishizuka, O., Taylor, R.N., Minshull, T.A. & Whitmarsh, R.B. 2008. Age of Seychelles–India break-up. *Earth and Planetary Science Letters*, **272**, 264–277.

Collier, J.S., Minshull, T.A., Hammond, J.O.S., *et al.* 2009. Factors influencing magmatism during continental breakup: New insights from a wide-angle seismic experiment across the conjugate Seychelles–Indian margins. *Journal of Geophysical Research: Solid Earth*, **114**, B03101, doi:10.1029/2008JB005898.

Corti, G. 2009. Continental rift evolution: from rift initiation to incipient break-up in the Main Ethiopian Rift, East Africa. *Earth-Science Reviews*, **96**, 1–53.

Corti, G., Bonini, M., Mazzarini, F., *et al.* 2002. Magma-induced strain localization in centrifuge models of transfer zones. *Tectonophysics*, **348**, 205–218.

Corti, G., Bonini, M., Conticelli, S., Innocenti, F., Manetti, P. & Sokoutis, D. 2003*a*. Analogue modelling of continental extension: a review focused on the relations between the patterns of deformation and the presence of magma. *Earth-Science Reviews*, **63**, 169–247.

Corti, G., Van Wijk, J., Bonini, M., Sokoutis, D., Cloetingh, S., Innocenti, F. & Manetti, P. 2003*b*. Transition from continental break-up to punctiform seafloor spreading: How fast, symmetric and magmatic. *Geophysical Research Letters*, **30**, 1604, doi:10.1029/2003GL017374.

Corti, G., Bonini, M., Sokoutis, D., Innocenti, F., Manetti, P., Cloetingh, S. & Mulugeta, G. 2004. Continental rift architecture and patterns of magma migration: a dynamic analysis based on centrifuge models. *Tectonics*, **23**, TC2012, doi:10.1029/2003TC001561.

Courtillot, V.E. & Renne, P.R. 2003. On the ages of flood basalt events. *Comptes Rendus, Géoscience*, **335**, 113–140.

Doglioni, C., Gueguen, E., Sàbat, F. & Fernandez, M. 1997. The western Mediterranean extensional basins and the Alpine orogen. *Terra Nova*, **9**, 109–112.

Dugda, M.T., Nyblade, A.A., Julia, J., Langston, C.A., Ammon, C.J. & Simiyu, S. 2005. Crustal structure in Ethiopia and Kenya from receiver function analysis: Implications for rift development in eastern Africa. *Journal of Geophysical Research: Solid Earth*, **110**, B01303, doi:1029/2004JB003065.

Eagles, G., Gloaguen, R. & Ebinger, C. 2002. Kinematics of the Danakil microplate. *Earth and Planetary Science Letters*, **203**, 607–620.

England, P. 1983. Constraints on extension of continental lithosphere. *Journal of Geophysical Research: Solid Earth*, **88**, 1145–1152.

Faccenna, C., Becker, T.W., Pio Lucente, F., Jolivet, L. & Rossetti, F. 2001. History of subduction and back-arc extension in the Central Mediterranean. *Geophysical Journal International*, **145**, 809–820.

Farnetani, C. & Richards, M.A. 1994. Numerical investigations of the mantle plume initiation model for flood basalt events. *Journal of Geophysical Research*, **99**, 13813–13833.

Fernàndez, M. & Ranalli, G. 1997. The role of rheology in extensional basin formation modelling. *Tectonophysics*, **282**, 129–145.

Frey, Ø., Planke, S., Symonds, P.A. & Heeremans, M. 1998. Deep crustal structure and rheology of the Gascoyne volcanic margin, western Australia. *Marine Geophysical Researches*, **20**, 293–312.

Gac, S. & Geoffroy, L. 2009. 3D thermo-mechanical modelling of a stretched continental lithosphere containing localised low-viscosity anomalies (the soft-point theory of plate break-up). *Tectonophysics*, **468**, 158–168.

Gaina, C., Gernigon, L. & Ball, P. 2009. Palaeocene–Recent plate boundaries in the NE Atlantic and the formation of the Jan Mayen microcontinent. *Journal of the Geological Society, London*, **166**, 601–616.

Garfunkel, Z. & Beyth, M. 2006. Constraints on the structural development of Afar imposed by the kinematics of the major surrounding plates. *In:* Yirgu, G., Ebinger, C.J. & Maguire, P.K.H. (eds) *The Afar Volcanic Province within the East African Rift System*. Geological Society, London, Special Publications, **259**, 23–42.

Gattacceca, J., Deino, A., Rizzo, R., Jones, D.S., Henry, B., Beaudoin, B. & Vadeboin, F. 2007. Miocene rotation of Sardinia: New paleomagnetic and geochronological constraints and geodynamic implications. *Earth and Planetary Science Letters*, **258**, 359–377.

Griffiths, R. & Campbell, I. 1991. Interaction of mantle plume heads with the Earth's surface and onset of small-scale convection. *Journal of Geophysical Research: Solid Earth*, **96**, 18295–18310.

Gudlaugsson, S.T., Gunnarsson, K., Sand, M. & Skogseid, J. 1988. Tectonic and volcanic events at the Jan Mayen Ridge microcontinent. *In:* Morton, A.C. & Parson, L.M. (eds) *Early Tertiary Volcanism and the Opening of the NE Atlantic*. Geological Society, London, Special Publications, **39**, 85–93.

Gueguen, E., Doglioni, C. & Fernandez, M. 1998. On the post-25 Ma geodynamic evolution of the western Mediterranean. *Tectonophysics*, **298**, 259–269.

Hamann, N.E., Whittaker, R.C. & Stemmerik, L. 2005. Geological development of the Northeast Greenland Shelf. *In:* Doré, A.G. & Vining, B.A. (eds) *Petroleum Geology: North-West Europe and Global Perspectives. Proceedings of the 6th Petroleum Conference*. Geological Society, London, 887–902.

Harry, D.L. & Leeman, W.P. 1995. Partial melting of melt metasomatized subcontinental mantle and the magma source potential of the lower lithosphere. *Journal of Geophysical Research: Solid Earth*, **100**, 10255–10269.

Jolivet, L., Faccenna, C., Goffé, B., *et al.* 1998. Midcrustal shear zone in

postorogenic extension: Example from the northern Tyrrhenian Sea. *Journal of Geophysical Research: Solid Earth*, **103**, 12123–12160.

Kasten, K.A., Mascle, J., Auroux, C., *et al.* 1988. ODP Leg 107 in the Tyrrhenian Sea: insights into passive margin and backarc basin evolution. *Geological Society of America Bulletin*, **100**, 1140–1156.

King, S.D. & Anderson, D.L. 1998. Edge-driven convection. *Earth and Planetary Science Letters*, **160**, 289–296.

Koch, P.S., Christie, J.M., Ord, A. & George, R.P., Jr. 1989. Effect of water on the rheology of experimentally deformed quartzite. *Journal of Geophysical Research: Solid Earth*, **94**, 13975–13996.

Kuvaas, B. & Kodaira, S. 1997. The formation of the Jan Mayen microcontinent: the missing piece in the continental puzzle between the Møre–Vøring Basins and East Greenland. *First Break*, **15**, 239–247.

Larsen, H.C. 1984. Geology of the East Greenland Shelf. *In:* Spencer, A.M., Hotter, E., Johnsen, S.O. *et al.* (eds) *Petroleum Geology of the North European Margin*. Graham & Trotman, London, 329–339.

Le Gall, B., Daoud, M.A., Maury, R.C., Rolet, J. & Guillou, H. 2010. Magma-driven antiform structures in the Afar rift: the Ali Sabieh range, Djibouti *Journal of Structural Geology*, doi: 10.1016/j.jsg.2010.06.007.

Lonergan, L. & White, N. 1997. Origin of the Betic–Rif mountain belt. *Tectonics*, **16**, 504–522.

Makris, J. & Ginzburg, A. 1987. The Afar Depression: transition between continental rifting and sea-floor spreading. *Tectonophysics*, **141**, 199–214.

Manighetti, I., Tapponnier, P., Gillot, P.Y., *et al.* 1998. Propagation of rifting along the Arabia–Somalia plate boundary: into Afar. *Journal of Geophysical Research: Solid Earth*, **103**, 4947–4974.

Masson, D.G. 1984. Evolution of the Macarene Basin, western Indian Ocean, and the significance of the Amirante Arc. *Marine Geophysical Researches*, **6**, 365–382.

Mauffret, A. & Contrucci, I. 1999. Crustal structure of the North Tyrrhenian Sea: first result of the multichannel seismic LISA cruise. *In:* Durand, B., Jolivet, L., Horváth, F. & Séranne, M. (eds) *The Mediterranean Basins: Tertiary Extension within the Alpine Orogen*. Geological Society, London, Special Publications, **156**, 169–193.

McKenzie, D.P. & Sclater, J.G. 1971. The evolution of the Indian Ocean since the Late Cretaceous. *Geophysical Journal of the Royal Astronomical Society*, **25**, 437–528.

Melosh, H.J. & Raefsky, A. 1980. The dynamical origin of subduction zone topography. *Geophysical Journal of the Royal Astronomical Society*, **60**, 333–354.

Melosh, H.J. & Raefsky, A. 1981. A simple and efficient method for introducing faults into finite element computations. *Bulletin of the Seismological Society of America*, **71**, 1391–1400.

Melosh, H.J. & Williams, C.A. 1989. Mechanics of graben formation in crustal rocks: a finite element analysis. *Journal of Geophysical Research: Solid Earth*, **94**, 13961–13973.

Menzies, M.A., Klemperer, S.L., Ebinger, C.J. & Baker, J. 2002. Characteristics of volcanic rifted margins. *In:* Menzies, M.A., Klemperer, S.L., Ebinger, C.J. & Baker, J. (eds) *Volcanic Rifted Margins*. Geological Society of America, Special Papers, **362**, 1–14.

Meyer, R., Van Wijk, J. & Gernigon, L. 2007. The North Atlantic Igneous Province: a review of models for its formation. *In:* Foulger, G.R. & Jurdy, D.M. (eds) *Plates, Plumes and Planetary Processes*. Geological Society of America, Special Papers, **430**, 525–552.

Mittelstaedt, E., Ito, G. & Behn, M.D. 2008. Mid-ocean ridge jumps associated with hotspot magmatism. *Earth and Planetary Science Letters*, **266**, 256–270.

Mjelde, T., Raum, T., Myhren, B., *et al.* 2005. Continent–ocean transition on the Vøring Plateau, NE Atlantic, derived from densely sampled ocean bottom seismometer data. *Journal of Geophysical Research: Solid Earth*, **110**, B05101, doi:10.1029/2004JB003026.

Mjelde, R., Raum, T., Breivik, A.J. & Faleide, J.I. 2008. Crustal transect across the North Atlantic. *Marine Geophysical Researches*, doi:10.1007/s11001-008-9046-9.

Müller, R.D., Gaina, G., Roest, W.R. & Hansen, D.L. 2001. A recipe for microcontinent formation. *Geology*, **29**, 203–206.

Müntener, O. & Manatschal, G. 2006. High degrees of melt extraction recorded by spinel harzburgite of the Newfoundland margin: The role of inheritance and consequences for the evolution of the southern North Atlantic. *Earth and Planetary Science Letters*, **252**, 437–452.

Negredo, A.M., Fernàndez, M. & Zeyen, H. 1995. Thermo-mechanical constraints on kinematic models of lithospheric extension. *Earth and Planetary Science Letters*, **134**, 87–98.

Norton, I.O. & Sclater, J.G. 1979. A model for the evolution of the Indian Ocean and the breakup of Gondwanaland. *Journal of Geophysical Research: Solid Earth*, **84**, 6803–6830.

Pérez-Gussinyé, M. & Reston, T.J. 2001. Rheological evolution during extension at nonvolcanic rifted margins: Onset of serpentinization and development of detachments leading to continental breakup. *Journal of Geophysical Research: Solid Earth*, **106**, 3961–3975.

Péron-Pinvidic, G. & Manatschal, G. 2008. The final rifting evolution at deep magma-poor passive margin from Iberia–Newfoundland: a new point of view. *International Journal of Earth Sciences*, doi:10.1007/s00531-008-0337-9.

Plummer, P.S. & Belle, E.R. 1995. Mesozoic tectonostratigraphic evolution of the Seychelles Microcontinent. *Sedimentary Geology*, **96**, 73–91.

Ranalli, G. 1995. *Rheology of the Earth*, 2nd edn. Chapman & Hall, London.

Reid, I. & Jackson, H.R. 1981. Oceanic spreading rate and crustal thickness. *Marine Geophysical Researches*, **5**, 165–172.

Sandwell, D.T. & Smith, W.H.F. 1997, Marine gravity anomaly from Geosat and ERS1 satellite altimetry. *Journal of Geophysical Research: Solid Earth*, **102**, 10039–10054.

Sengör, A.M.C. & Burke, K. 1978. Relative timing of rifting and volcanism on Earth and its tectonic implications. *Geophysical Research Letters*, **5**, 419–421.

Shelton, G. & Tullis, J. 1981. Experimental flow laws for crustal rocks. *EOS Transactions, American Geophysical Union*, **62**, 396.

Skogseid, J., Planke, S., Faleide, J.I., Pedersen, T., Eldholm, O. & Everdal, F. 2000. NE Atlantic continental rifting and volcanic margin formation. *In:* Nøttvedt, A., Brekke, H., Birkeland, Ø., *et al.* (eds) *Dynamics of the Norwegian Margin*. Geological Society, London, Special Publications, **167**, 295–326.

Sparks, D.W. & Parmentier, E.M. 1991. Melt extraction from the mantle beneath spreading centers. *Earth and Planetary Science Letters*, **105**, 368–377.

Spohn, T. & Schubert, G. 1982. Convective thinning of the lithosphere: A mechanism for initiation of continental rifting. *Journal of Geophysical Research: Solid Earth*, **87**, 4669–4681.

Subrahmanya, K.R. 1998. Tectono-magmatic evolution of the west coast of India. *Gondwana Research*, **1**, 319–327.

Takeshita, T. & Yamaji, A. 1990. Acceleration of continental rifting due to a thermomechanical instability. *Tectonophysics*, **181**, 307–320.

Talwani, M. & Reif, C. 1998. Laxmi Ridge—A continental sliver in the Arabian Sea. *Marine Geophysical Researches*, **20**, 259–271.

Tegner, C., Brooks, C.K., Duncan, R.A., Heister, L.E. & Bernstein, S. 2008. ^{40}Ar–^{39}Ar ages of intrusions in East Greenland: Rift-to-drift transition over the Iceland hotspot. *Lithos*, **101**, 480–500.

Todal, A. & Edholm, O. 1998. Continental margin off Western India and Deccan Large Igneous Province. *Marine Geophysical Researches*, **20**, 273–291.

Van Wijk, J.W. & Cloetingh, S.A.P.L. 2002. Basin migration caused by slow lithospheric extension. *Earth and Planetary Science Letters*, **198**, 275–288.

Van Wijk, J.W., Huismans, R.S., Ter Voorde, M. & Cloetingh, S.A.P.L. 2001. Melt generation at volcanic continental margins: No need for a mantle plume? *Geophysical Research Letters*, **28**, 3995–3998.

White, R.S. & McKenzie, D.P. 1989, Magmatism at rift zones: the generation of volcanic continental margins and flood basalts. *Journal of Geophysical Research*, **94**, 7685–7729.

White, R.S. & Smith, L.K. 2009. Crustal structure of the Hatton and the conjugate east Greenland rifted volcanic continental margins, NE Atlantic. *Journal of Geophysical Research: Solid Earth*, **114**, B02305, doi:10.1029/2008JB005856.

Wilks, K.R. & Carter, N.L. 1990. Rheology of some continental lower crustal rocks. *Tectonophysics*, **182**, 57–77.

Yamada, Y. & Nakada, M. 2006. Stratigraphic architecture of sedimentary basin induced by mantle diapiric upwelling and eustatic event. *Tectonophysics*, **415**, 103–121.

Yamasaki, T. & Gernigon, L. 2009. Styles of lithospheric extension controlled by underplated mafic bodies. *Tectonophysics*, **468**, 169–184.

Yamasaki, T., Miura, H. & Nogi, Y. 2008. Numerical modelling study on the flexural uplift of the Transantarctic Mountains. *Geophysical Journal International*, **174**, 377–390.

Yatheesh, V., Bhattacharya, G.C. & Dyment, J. 2009. Early oceanic opening off Western India–Pakistan margin: The Gop Basin revisited. *Earth and Planetary Science Letters*, **284**, 399–408.

Yuen, D.A. & Fleitout, L. 1985. Thinning of the lithosphere by small-scale convective destabilization. *Nature*, **313**, 125–128.

Received 12 February 2010; revised typescript accepted 2 June 2010.
Scientific editing by Ken McCaffrey.